



SL14

## STUDY OF EXPERIMENTALLY DYNAMICALLY COMPRESSED DOLOMITE USING TEM AND X-RAY POWDER DIFFRACTION

R. Skála<sup>1</sup>, N. Miyajima<sup>2</sup>, F. Langenhorst<sup>3</sup> and F. Hörz<sup>4</sup>

<sup>1</sup>Geologický ústav AVČR, v.v.i., Rozvojová 269, 16500 Praha

<sup>2</sup>Bayerisches Geoinstitut, Universität Bayreuth, D-95440 Bayreuth, Germany

<sup>3</sup>Institut für Geowissenschaften, Bereich Mineralogie, Friedrich-Schiller-Universität Jena, Fürstengraben 1, D-07743 Jena, Germany

<sup>4</sup>SN2, NASA Johnson Space Center, Houston, TX 77058, USA

The response of carbonate-dominated sediments to transient strong dynamic compression and subsequent rapid unloading is essential for understanding atmospheric CO<sub>2</sub> pollution and environmental consequences of large-scale asteroid impacts on the Earth. The experimental data on the deformation behavior of dolomite under strong dynamic (i.e., shock) compression are scarce and the threshold shock pressures and temperatures for partial to complete decomposition are completely missing.

Consequently, we have carried out shock-recovery experiments at the Johnson Space Center, NASA, Houston, USA, using a 20-mm-caliber powder propellant gun. The starting material was a dense (~ 0.04% porosity) dolomite rock composed of equi-granular grains, typically 25 μm across. Pressures attained by multiple shock reverberation technique covered the range from 4 to 61 GPa (Table 1). To characterize the shock defects over the entire range of conditions we prepared five shock-loaded samples (20, 25, 29,

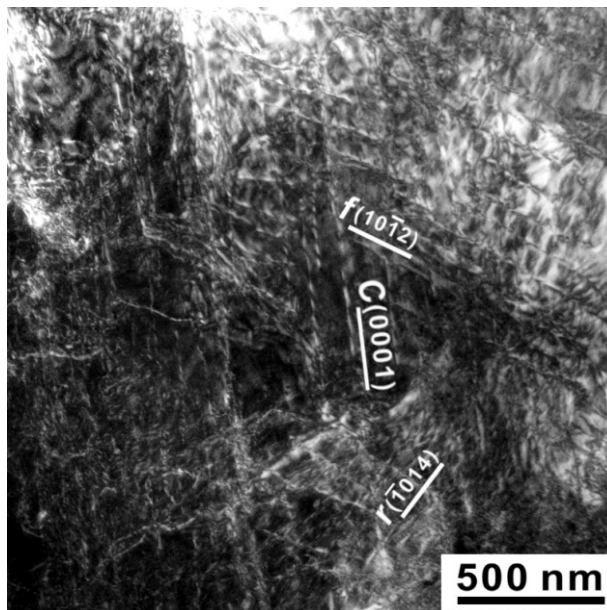


**Fig. 1.** Weak-beam dark-field image of dislocations of *f*-, *c*- and *r*-slip systems.

**Table 1.** Summary of shock recovery experiments indicating the pressures attained on the cover plate/flyer plate (CP/FP) interface and in the sample (in GPa).

Shot #	$v_i$ (km/s)	Material	Pressure (GPa)		
			Flyer	Cover	CP /FP sample
2064	1.131	Lexan	Al2024	4.2	4.2
2065	1.694	Lexan	SS304	7.4	7.4
2066	1.345	Al2024	SS304	17.0	17.0
2067	1.371	Al2024	SS304	17.4	17.4
2068	1.34	SS304	SS304	28.8	28.8
2069	1.478	Al2024	SS304	19.0	19.0
2070	1.54	Al2024	SS304	20.0	20.0
2071	1.121	SS304	SS304	23.5	23.4
2072	1.192	SS304	SS304	25.2	25.1
2073	1.345	Al2024	SS304	18.8	18.8
2094	1.26	W	FS77	55.0	43.1
2096	1.413	SS304	FS77	42.7	42.3
2097	1.461	W	FS77	65.4	51.6
2099	1.533	W	FS77	69.0	61.2

42 and 61 GPa) and the undeformed starting material for TEM observation.

Deformation features recorded in shock-loaded dolomite samples include perfect and partial dislocations, stacking faults, and microtwins. Dislocations are omnipresent in all samples; they are already present in the unshocked starting material but their density significantly increases with shock pressure. Highest dislocations densities on the order of  $10^{14} \text{ m}^{-2}$  are observed in samples shocked to medium to high shock pressures (30 – 61 GPa). At lower pressures (< 30 GPa), *c*-type dislocations dominate; at higher pressures (> 30 GPa), *f*- and *r*-type dislocations become more important though *c*-type dislocations are still present (Fig. 1). Distinct narrow twin lamellae on *f*-planes occur exclusively in the sample shocked to 42 GPa. Partial dislocations were observed in the twin walls, indicating their mechanical nature. Stacking faults occur in all samples, however, they are more frequent in materials shocked to higher pressures. The sample shocked to 61 GPa shows weak diffuse streaks or superstructure reflections in selected area electron diffraction patterns, which might be the result of cation disordering at high post-shock temperatures (Fig. 2).

In powder diffraction patterns, the most notable feature is a systematic broadening of the peaks with increasing peak shock pressure due to an increase of micro-strain and decrease in size of coherently diffracting domains. The unit-cell dimensions systematically increased by  $\sim 0.5\%$  at 30 GPa; at still higher pressures, cell size remains invariant. The diffraction data, in agreement with those obtained by TEM, do not indicate decomposition of dolomite under even the highest dynamic loads.

In summary, the defect microstructures document strong deformation of dolomite under dynamic compression with high strain-rates but features indicating significant outgassing or melting were not observed in dolomite shock-loaded to the pressures as high as 61 GPa. These results indicate that decomposition may only be possible if the porosity of starting materials were high or if shock pressures were much higher.

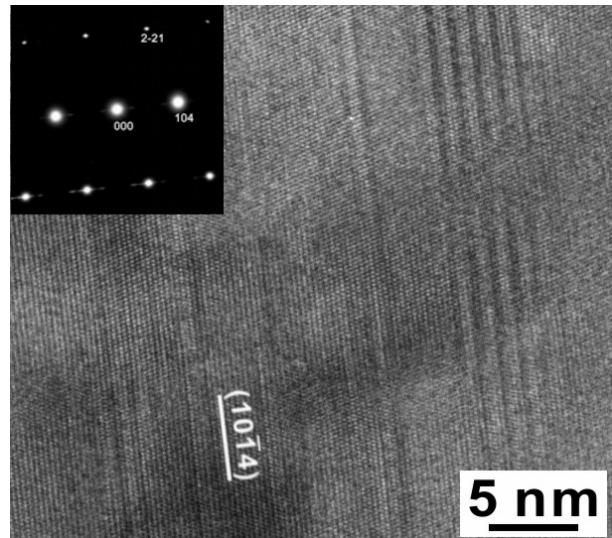


**Fig. 2.** High resolution TEM image of the sample shocked to 61 GPa, indicating some stacking faults along the (10-14) plane. The inset is the selected area electron diffraction pattern illustrating weak diffuse streaks.

SL15

## MSTRUCT EXTENSION FOR LINE PROFILE ANALYSIS OF INDIVIDUAL DIFFRACTION PEAKS – APPLICATION TO MATERIALS WITH ANISOTROPIC LINE BROADENING

Z. Matěj<sup>1</sup>, T. Brunátová<sup>1</sup>, L. Matějová<sup>2,3</sup>, V. Valeš<sup>1,4</sup>, D. Popelková<sup>5</sup>, R. Kužel<sup>1</sup>

<sup>1</sup>Faculty of Mathematics and Physics, Charles University in Prague,  
Ke Karlovu 5, 121 16 Praha 2, Czech Republic

<sup>2</sup>VŠB-Technical University of Ostrava, 17. listopadu 15, Ostrava – Poruba

<sup>3</sup>Institute of Chemical Process Fundamentals of the ASCR, v.v.i., Rozvojova 2, Praha 6

<sup>4</sup>J. Heyrovsky Institute of Physical Chemistry of the ASCR, v.v.i., Dolejškova 3, Praha 8

<sup>5</sup>Institute of Macromolecular Chemistry of the ASCR, v. v. i., Heyrovského nám. 2, Praha 6  
matej@karlov.mff.cuni.cz

**Keywords:** XRD, anisotropy, strain, nanorods

### Abstract

Application of an extension of the MSTRUCT powder diffraction software for refinement of individual diffraction line profile parameters is illustrated on the case studies of nanocrystalline anatase TiO<sub>2</sub> particles, Na<sub>2</sub>Ti<sub>6</sub>O<sub>13</sub> titanate nanorods and CeTi<sub>2</sub>O<sub>6</sub> titanate samples with strong anisotropic size and strain diffraction line broadening.

### Introduction

The *Rietveld* and *whole powder pattern modelling* (WPPM) methods [1] are the most common approaches used for powder diffraction analysis nowadays. They can profit from general as well as material specific structural models and overcome the peak overlap problem. This is especially true for low symmetry and multiphase materials. Due to complexity of these methods it can be difficult to understand how particular model parameters are related to experimental data. This is less difficult within the methods of analysis of individual lines, such as the *Williamson-Hall* plot method or without restrictions to line profile analysis (LPA) also e.g. the *sin<sup>2</sup>( $\psi$ ) method*. They offer direct relation between relevant effects in experimental data and

model parameters. Unfortunately peak overlap or other difficulties can limit their applicability.

An extension of the Rietveld/WPPM like MSTRUCT software [2] for refinement of profile parameters of individual diffraction peaks is presented. With this extension it is possible to switch off particular physical effects for individual *hkl* diffraction lines. On the contrary additional pseudo-Voigt profiles can be included in the convolution kernel for these reflections. In this way additional peak shifts or broadening effects can be introduced for specific (strong or not overlapped) diffraction lines whereas the rest of the pattern can be described by a more general “average” (micro)structural model. This is especially useful for fitting diffraction patterns with many peaks from low symmetry and multiphase materials. The refined *hkl* parameters (shifts, line widths etc.) can later be analysed by other methods. Similar features are available also in TOPAS [3] or Pm2K [4] software.

Crystal properties are anisotropic in nature. This is reflected in dependence of diffraction line parameters on *hkl* indexes and sample orientation. This anisotropy can be a principal footprint which reveals the presence and nature of important (micro)structure aspects of the studied material, e.g. the presence of specific defects (dislocations, planar



```

natio.imp

56 // the 1st phase - strange effects
57 HKLpVoigtA      HKLeNa2Ti6O13      broadening component type (pVoigt(A),SizeLn,dislocSLvB,HKLpVoigtA)
58

Phkl_HKLeNa2Ti6O13.dat

1 # Tue Feb 18 19:22:52 2014
2 #   h   k   l   func   dtth(deg) fixed   fwhm(deg) fixed   eta fixed   asym fixed   disabled-effects
3   2   0   0   pV     0.0475  0     0.236  0   0.80  0   1.00  1   all_not_instr
4  -2   0   1   pV    -0.0263  0     0.214  0   0.61  0   1.00  1   all_not_instr
5   ...
6   0   2   0   pV     0.0000  1     0.086  0   0.40  0   1.00  1   all_not_instr
7   ...
8 #
9 @local_bkg_chebyshev  10.500  15.500  3  -1.428e+03 0  -7.841e+03 0  0.000e+00 1
10 @local_bkg_chebyshev  22.700  26.000  3  2.769e+03 0  1.454e+04 0  0.000e+00 1
11 ...
12 @end
  
```

**Figure 1.** Definition of the MSTRUCT “HKLpVoigtA” effect for fitting of individual *hkl* lines. It contains line profile parameters (dtth-shift, fwhm, eta, asym) and definition of local backgrounds (in the bottom).

faults), crystallites shape anisotropy or a presence of residual stresses.

The *Williamson-Hall* plot method with LPA parameters refined using the MSTRUCT extension was applied to (1) anatase TiO<sub>2</sub> nanoparticles and (2) Na<sub>2</sub>Ti<sub>6</sub>O<sub>13</sub> and (3) CeTi<sub>2</sub>O<sub>6</sub> titanates.

### MSTRUCT extension for refinement of individual *hkl* profile parameters

In MSTRUCT there was a possibility to include additional position and broadening correction for individual *hkl* lines already earlier (before 2013) within the “HKLpVoigtA” effect. Recently the effect was extended with options to save the profile parameters into a separate file (Fig. 1) and switch off specific effects for arbitrary *hkl*. Usually a general model is used to fit the most of the powder pattern. For few selected *hkl* reflections of the crystalline phase under study these general models are switched off, with an exception of the instrumental broadening, and an additional phenomenological pseudo-Voigt profile can be included (Fig. 1). The refined profile parameters can be later visualized and analysed by other software.

### Application to anatase nanoparticles

The method was applied to nanocrystalline TiO<sub>2</sub> samples prepared by hydrolysis of titanium alkoxides and subsequent calcination [5,6]. The dominant crystalline phase – anatase – can form bipyramidal crystals truncated by (001) lattice planes [6,7]. This would induce strong anisotropic line broadening [6], which is however not observed for the studied samples. It was shown for a certain ratio of (101) and (001) facets the broadening is close to isotropic and simple model of spherical crystallites can be used [6,7].

### Na<sub>2</sub>Ti<sub>6</sub>O<sub>13</sub> titanate nanorods

The full potential of the MSTRUCT extension was utilized in the analysis of powder patterns from sodium-titanate nanorods formed by thermal heating of titanate nanotubes [8] (above 850°C). Beside the main titanate phase with about 100 reflections there are strong peaks from anatase and rutile phases in the experimental patterns. This complicates extraction of line profile parameters. Nevertheless it is evident in the measured patterns that broadening effects

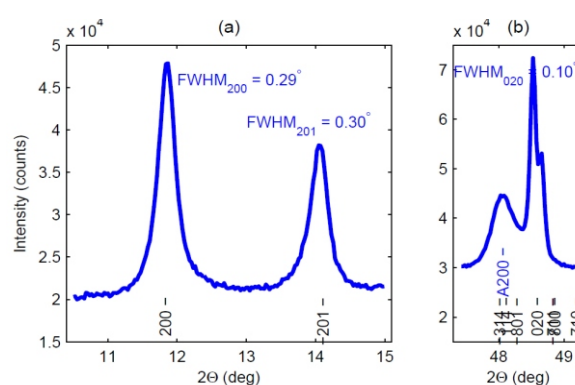


**Figure 2.** Parts of the measured diffraction pattern of a sodium-titanate nanotubes sample heated at 850°C for 105 min in air.

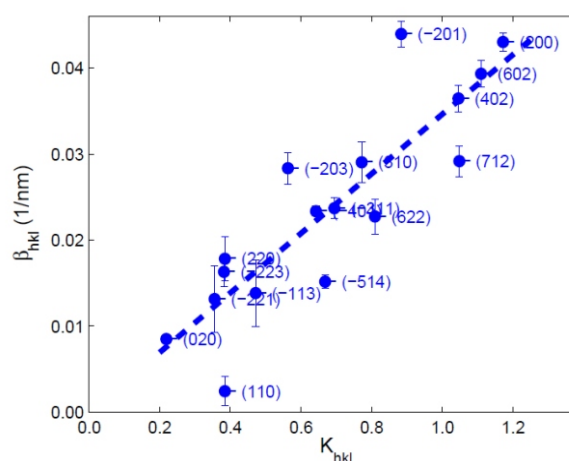


**Figure 3.** Integral line widths ( $\beta_{hkl}$ ) of selected Na<sub>2</sub>Ti<sub>6</sub>O<sub>13</sub> diffraction lines plotted vs. the Scherrer constant ( $K_{hkl}$ ) for the model of rod-like crystallites with oval basis [8].

are strongly anisotropic (Fig. 2, 3) and the effect is related to nature of this material to form nanorods with axis parallel to the crystal monoclinic axis [8].

### Anisotropic strain broadening in CeTi<sub>2</sub>O<sub>6</sub> titanates

Contrary to two previous cases in CeTi<sub>2</sub>O<sub>6</sub> titanate samples prepared by heating of sol-gel Ti-Ce mixed oxides at temperatures above 750°C the anisotropic strain broadening

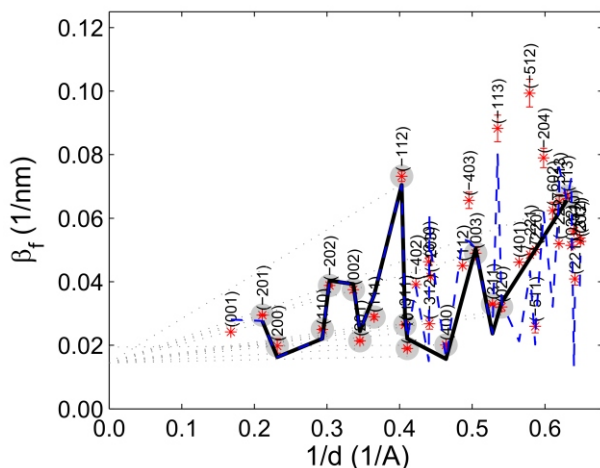


**Figure 4.** Williamson-Hall plot for selected  $\text{CeTi}_2\text{O}_6$  diffraction lines. Shadow circles mark reliable  $hkl$  widths which were used for an initial guess (black line) of parameters of the Popa anisotropic strain broadening model. Blue dashed line shows a dependence of model predicted widths for other analysed reflections.

was the dominant effect [9] (Fig. 4). It was possible to describe this effect by the phenomenological model developed by Popa [10]. According to this model the microstrain ( $e_{hkl}$ ) is described by 9 model parameters ( $E_1, \dots, E_9$ ) [10]

$$e_{hk}^2 = \frac{e_{hh}^2 (E_1 h^4 + E_2 l^4 + E_3 k^4 + 2E_4 h^2 l^2 + 2E_5 l^2 k^2 + 2E_6 h^2 k^2 + 4E_7 h^3 l + 4E_8 l^3 h + 4E_9 k^2 l) / (H_{hkl} a)^4}{}, \quad (1)$$

where  $H_{hkl} = 1/d_{hkl}$  is the diffraction vector length, “ $a$ ” is the lattice parameter and  $e_{hh}$  is an additional microstrain scaling parameter.

## Summary

The presented MSTRUCT extension can be utilized for refinement of individual  $hkl$  lines profile parameters in whole diffraction patterns from low symmetry or multiphase materials with many overlapped reflections. Specific size

broadening models accounting for natural crystal shapes were used to describe size broadening in case of anatase nanoparticles and sodium-titanate nanorods. Anisotropic microstrain in  $\text{CeTi}_2\text{O}_6$  titanate samples was described by the phenomenological model of Popa. The case studies here illustrate that analysis of individual diffraction lines and the whole pattern modeling approach are complementary methods. The former one offers a qualitative description, ideas and initial parameters for the starting model. The later method gives qualitative results.

## References

1. P. Scardi, M. Leoni, *Acta Cryst. A*, **58**, (2002), 190.
2. Z. Matěj, R. Kužel, *MSTRUCT*, [www.xray.cz/mstruct](http://www.xray.cz/mstruct) (May 20, 2014).
3. Coelho software, *TOPAS Academic*, [www.topas-academic.net](http://www.topas-academic.net) (May 20, 2014).
4. M. Leoni, T. Confente, P. Scardi, *Z. Kristallogr. Suppl.*, **23**, (2006), 249.
5. L. Matějová, Z. Matěj, O. Šolcová, *Micro. Mesoporo. Materials*, **154**, (2012), 187.
6. Z. Matěj, L. Matějová, R. Kužel, *Pow. Diffr.*, **28**, (2013), S161.
7. Z. Matěj, R. Kužel, *Materials Struct. Chem. Biol. Phys. Tech.*, **19**(2), (2012), 121, [www.xray.cz/mstruct](http://www.xray.cz/mstruct).
8. T. Brunatová, Z. Matěj, P. Oleynikov, S. Daniš, D. Popelková, X. Zou, R. Kužel, submitted to *Mater. Character.* (Feb 2014).
9. V. Valeš, L. Matějová, Z. Matěj, T. Brunatová, V. Holý, *J. Phys. Chem. Sol.*, **75**, (2014), 265.
10. N. C. Popa, *J. Appl. Cryst.*, **31**, (1998), 176.

## Acknowledgements

This work has been supported by the Grant Agency of the Czech Republic (project no. 14-23274S) and within the Charles University Research Center “Physics of Condensed Matter and Functional Materials” (no. UNCE 204023/2012).

SL16

## AUXILIARY PROGRAMS FOR DIFFRACTION EXPERIMENTS

Jiří Čapek<sup>1</sup>, Zdenek Pala<sup>1, 2</sup>

<sup>1</sup>Department of Solid State Engineering, Faculty of Nuclear Sciences and Physical Engineering, Czech Technical University in Prague

<sup>2</sup>Institute of Plasma Physics, Academy of Sciences of the Czech Republic  
capekjir@jfifi.cvut.cz

Because of recurring pleas of colleagues who are frequent users of X-ray diffraction results and who wanted to know the relevant volume of material which was irradiated, programs for calculation of penetration depth and linear absorption coefficients of crystalline phases were written in MatLab environment. In addition to it, we were often faced with oddly positioned Debye rings obtained in back reflection experiment. Debye rings’ convenient location on area, 2D, detector was, thus, achieved by repeatedly performing

the experiments. That had led us to create a program which would visualize the outcome for selected experimental parameters.

*Debye* software was created as a visual aid for users doing the so called the back reflection experiment (or back-scattering Debye-Scherrer experiment) [1]. It is a basic method for qualitative determination of real structure of materials. In materials only planes, which are oriented in the manner satisfying the Bragg’s law, can diffract. The

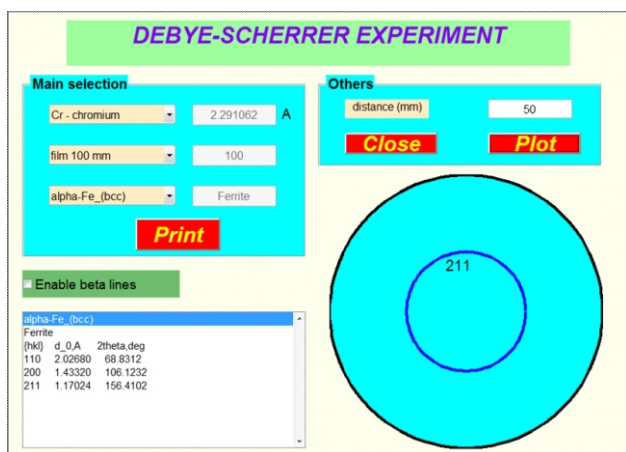


Figure 1. User interface of the *debye* software.

diffracted radiation has a character of diffraction cones with the apex angle of  $4^\circ$ . If this diffracted radiation impacts on a 2D detector, the so called Debye rings are detected. The user can make a model of the experiment upon changing the experimental parameters and also can check an expected result for untextured polycrystalline fine-grained materials. This is especially helpful for setting the right distance between the irradiated sample and 2D detector when the dimension of the detector is known. In Fig. 1, there is the result for standard alpha-ferrite steel in the distance of 50 mm from the detector when radiation from X-ray tube with chromium anode is used.

*Absorption coefficient* software was created because it is de rigueur to know the values of linear absorption/attenuation coefficients when the penetration depth is to be calculated since it describes the reduction of an energy beam upon passing through a specific material [2]. For calculation of a linear absorption coefficient it is necessary to know the amount of each phase in material, densities and chemical formulas of the phases. In Fig. 2, there is the user interface of the program with the result of alpha-ferrite steel with oxidation layer (again for CrK radiation). This constant is subsequently applied in the calculation of corresponding penetration depth as seen in Fig. 3.

X-ray penetration depth software was created because the users of XRD results must be informed about the volume of the material to which the results are relevant. Irradiated volume is given by irradiated surface, defined by experimental set-up and the inserted slits, multiplied by penetration depth. Most commonly, the penetration depth is represented by values of the so called *effective penetration depth*  $T^{ef}$  which defines the thickness of surface layer that gives rise to 63 % of diffracted intensity [1]. Hence, this software provides the opportunity to furnish users with  $T^{ef}$  values, or courses, for the given radiation penetrating the irradiated material. Final values generally depend on an incidence, a rebound angle and on an absorption coefficient. The user can choose between four types of experimental set-up. Except for standard Bragg-Brentano geometry and grazing incidence diffraction, courses of  $T^{ef}$  during residual-stress-aimed diffraction experiment for diffractometer can be visualized for all measured tilts and  $T^{ef}$  for  $\omega$ -scans can be plotted as well [3]. User interface of this program is in Fig. 3 on the left while on the right; there

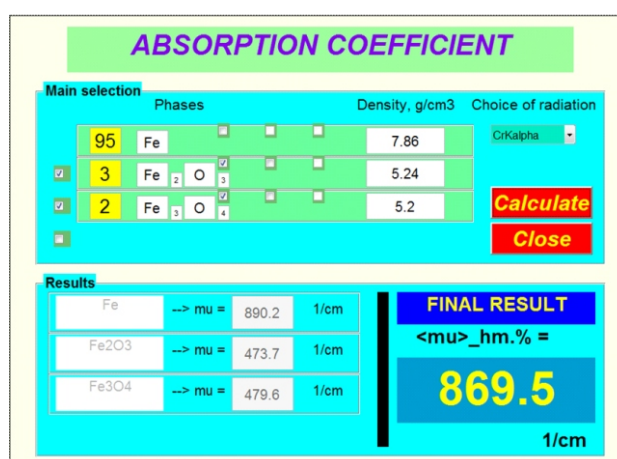


Figure 2. User interface of the *absorption coefficient* software.

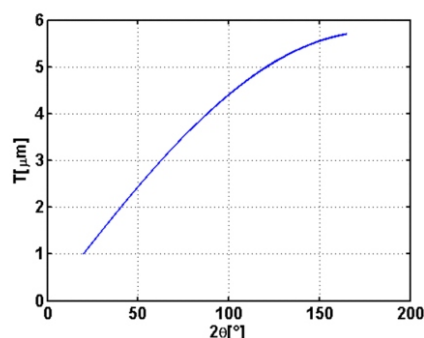
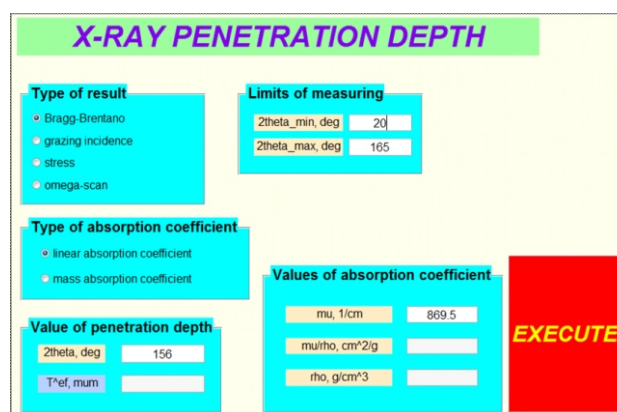


Figure 3. User interface of the *X-ray penetration depth* software.

is the result of  $T^{ef}$  course for linear absorption coefficient calculated above and Bragg-Brentano geometry.

The programs are available for users who have at their disposal MatLab from <http://electron.fjfi.cvut.cz/drupal/software-laborator-strukturni-rentgenografie>.

1. I. Kraus, N. Ganev, *Difrakční analýza mechanických napětí*. Praha: ČVUT, 1995. ISBN 80-01-01366-9.
2. B. D. Cullity, S. R. Stock, *Elements of X-ray Diffraction*. New Jersey: Prentice Hall, 2001. ISBN 0-201-61091-4.
3. M. Birkholz, *Thin Film Analysis by X-ray Scattering*. Weinheim: WILEY-VCH, 2006. ISBN 978-3-527-31052-4.

This work was supported by the Grant Agency of the Czech Technical University in Prague, grant No. SGS13/219/OHK4/3T/14.